



UNIVERSITY OF LEEDS

This is a repository copy of *Magnetic field tunable terahertz quantum well infrared photodetector*.

White Rose Research Online URL for this paper:
<http://eprints.whiterose.ac.uk/1117/>

Article:

Savic, I., Milanovic, V., Vukmirovic, N. et al. (4 more authors) (2005) Magnetic field tunable terahertz quantum well infrared photodetector. *Journal of Applied Physics*, 98 (8). 084509-(8 pages). ISSN 1089-7550

<https://doi.org/10.1063/1.2085309>

Reuse

See Attached

Takedown

If you consider content in White Rose Research Online to be in breach of UK law, please notify us by emailing eprints@whiterose.ac.uk including the URL of the record and the reason for the withdrawal request.



eprints@whiterose.ac.uk
<https://eprints.whiterose.ac.uk/>



White Rose Consortium ePrints Repository

<http://eprints.whiterose.ac.uk/>

This is an author produced version of a paper published in **Journal of Applied Physics**.

White Rose Repository URL for this paper:
<http://eprints.whiterose.ac.uk/archive/00001117/>

Published paper

Savic, I. and Milanovic, V. and Vukmirovic, N. and Jovanovic, V.D. and Ikonic, Z. and Indjin, D. and Harrison, P. (2005) *Magnetic field tunable terahertz quantum well infrared photodetector*. *Journal of Applied Physics*, 98 (8). 084509-(8 pages).

Repository paper

Savic, I. and Milanovic, V. and Vukmirovic, N. and Jovanovic, V.D. and Ikonic, Z. and Indjin, D. and Harrison, P. (2005) *Magnetic field tunable terahertz quantum well infrared photodetector*.

Author manuscript available at: <http://eprints.whiterose.ac.uk/archive/00001117/>

Magnetic field tunable terahertz quantum well infrared photodetector

Ivana Savić¹, Vitomir Milanović^{2,1}, Nenad Vukmirović¹,

Vladimir D. Jovanović¹, Zoran Ikonić¹, Dragan Indjin¹, Paul Harrison¹

¹*School of Electronic and Electrical Engineering,*

University of Leeds, Leeds LS2 9JT, United Kingdom

²*Faculty of Electrical Engineering, University of Belgrade,*

11120 Belgrade, Serbia and Montenegro

Abstract

A theoretical model and a design of a magnetic field tunable CdMnTe/CdMgTe terahertz quantum well infrared photodetector are presented. The energy levels and the corresponding wavefunctions were computed from the envelope function Schrödinger equation using the effective mass approximation and accounting for Landau quantization and the giant Zeeman effect induced by magnetic confinement. The electron dynamics were modeled within the self-consistent coupled rate equations approach, with all relevant electron-longitudinal optical phonon and electron-longitudinal acoustic phonon scattering included. A perpendicular magnetic field varying between 0 T and 5 T, at a temperature of 1.5 K, was found to enable a large shift of the detection energy, yielding a tuning range between 24.1 meV and 34.3 meV, equivalent to 51.4 μm to 36.1 μm wavelengths. For magnetic fields between 1 T and 5 T, when the electron population of the QWIP is spin-polarized, a reasonably low dark current of $\leq 1.4 \times 10^{-2}$ A/cm² and a large responsivity of 0.36 – 0.64 A/W are predicted.

I. INTRODUCTION

In recent years there has been an increasing interest, and a considerable experimental and theoretical activity focused on dilute magnetic semiconductors (DMSs) whose unconventional properties offer a great prospect for developing a wide range of novel devices¹⁻⁶. The key reason for employing them in both basic and application-oriented research is the control of spin splitting that can be achieved by varying the material composition, an external magnetic field, temperature and/or via quantum confinement^{7,8}. These extensive studies have been conducted mostly in the area of spintronics, towards realization of spin-based devices¹⁻⁴. Some of the research activity has been oriented into the investigation of the spin splitting effects on interband transitions and the applications of DMSs in interband devices⁹⁻¹². On the contrary, very few studies aiming towards novel intersubband devices based on DMSs have been reported¹³.

In spite of significantly improved performance and technological advances of quantum well infrared photodetectors (QWIPs)¹⁴ and quantum cascade lasers (QCLs)¹⁵, they are still attracting a considerable amount of research attention. Different designs of QWIPs¹⁶⁻¹⁹, theoretical models of electron transport²⁰⁻²³ and various applications^{24,25} have been proposed. QCL operation has been recently demonstrated in the far-infrared range up to $160\mu\text{m}$ ²⁶⁻²⁹. The development of terahertz (THz) QCLs has motivated the research leading to development of THz QWIPs³⁰⁻³². Recently, the experimental observations of greatly improved GaAs/AlGaAs QCL performance under an applied magnetic field, in terms of threshold current and its temperature dependence, have been reported^{29,33,34}.

However, one of the much sought after improvements of THz QWIPs comprising doped symmetric rectangular quantum wells is external tunability. Magnetic field appears to offer great potential for tuning, if applied on structures based on DMSs. Due to the manipulation of the electronic structure by varying magnetic field, one can change the transition energies of the absorbed radiation¹³. Variations of a few meV which are achievable in CdMnTe (a DMS compound) imply a large tunability on a relative scale if the transition energy is in the THz range.

The aim of the present work is to explore the design of a magnetically tunable THz QWIP comprising CdMnTe/CdMgTe materials. Additionally, introducing a new material system for QWIPs offers a possibility to access the GaAs Reststrahlen region of 34 – 36 meV. A

model of electron transport in QWIPs in a magnetic field is then required in order to predict the QWIP output characteristics.

The organization of the paper is as follows. In Sec. II a theoretical model of QWIPs in a magnetic field is presented. The calculation of the electronic structure (energy levels and wavefunctions) of DMS quantum structures is described in Sec. IIA. The interaction of electrons with electromagnetic radiation in an external magnetic field in the dipole approximation is reviewed in Sec. IIB. The scattering rates between Landau levels due to the interaction with optical and acoustic phonons are given in Sec. IIC. Eventually, the rate equation model of QWIPs subjected to a magnetic field is presented in Sec. IID. The details of design and the results are presented in Sec. III. The tuning range of the QWIP in a magnetic field up to 5 T and the variation of the electron distribution are presented in Sec. IIIA and Sec. IIIB, respectively. The dark current and responsivity versus magnetic and electric field dependences are discussed in Sec. IIIC and Sec. IIID.

II. THEORETICAL CONSIDERATIONS

A. Electronic structure of DMS quantum wells

The unique properties of DMSs arise from their band structure with two distinct electronic subsystems: delocalized, band electrons and magnetic impurity electrons with magnetic moments localized in ionic open $3d$ (or $4f$) shell. The mobile electrons determine the electrical and optical properties of DMSs, while the localized magnetic moments are responsible for their magnetic properties. However, the unique magneto-optical properties of DMSs result from the strong spin-dependent $sp-d(f)$ exchange interactions between these two subsystems⁵⁻⁸.

Application of a perpendicular magnetic field to nonmagnetic semiconductor quantum wells splits the in-plane continuum of quantized subbands into Landau levels, each subband producing a set of Landau levels, described by a Landau index and additionally by spin index (gyromagnetic spin splitting within Landau levels)³⁵. Both the Landau level energies and their separation depend linearly on the magnetic field. If the structure includes a DMS, the conduction band edge varies with the magnetic field locally due to the $sp-d$ interaction, and hence modifies the potential profile. The shift of the potential (in the magnetic layers

and near the interfaces) is opposite for the two spins, and consequently they experience two different potential profiles, which are both a function of the magnetic field^{5,9,10,36}. This spin dependent variation of the confinement energy is particularly significant in the vicinity of the interfaces^{10,36} and in turn leads to different, and field-dependent, spectra for the two spins. This phenomenon is known as the giant Zeeman effect. Since the spin and Landau level index are conserved in optical transitions caused by z -polarized light, the transition energies will vary with the magnetic field. This translates into tunability of the intersubband transition energies by varying the magnetic field.

The total Hamiltonian of an electron in DMSs, in addition to the conventional Hamiltonian for nonmagnetic semiconductor structures, contains the spin-dependent potential induced by the magnetic field, given by an empirical expression^{5,9,10,36}

$$U_{DMS} = \pm \frac{1}{2} \alpha N_0 \bar{x} \langle S_z \rangle, \quad (1)$$

where “+” holds for spin-up and “-” for spin-down electrons, α is the sp - d exchange integral for the conduction band, N_0 is the density of cations, $\langle S_z \rangle$ is the thermal average of the Mn^{2+} spin, which, for paramagnetic materials, amounts to

$$\langle S_z \rangle = \frac{5}{2} B_{5/2} \left[\frac{5g^* \mu_B B}{2k(T + T_0)} \right], \quad (2)$$

where g^* is the Landé factor of the conduction band electrons (here assumed constant throughout the structure, $g^*(z) \approx 2$), μ_B is the Bohr magneton, B is the magnetic field along the z axis (the direction of confinement), k is the Boltzmann constant, T the temperature and $B_{5/2}$ is the Brillouin function

$$B_{5/2}(w) = \frac{6}{5} \coth\left(\frac{6}{5}w\right) - \frac{1}{5} \coth\left(\frac{1}{5}w\right). \quad (3)$$

Phenomenological fitting parameters \bar{x} and T_0 represent the effective manganese concentration and the effective temperature^{5,9,10,36} and both depend on the manganese concentration and the position on the z axis if the influence of a graded nonDMS/DMS interface and the enhanced magnetization in its vicinity is accounted for. A theoretical method mapping the detailed interface profile was used to obtain spatial and manganese concentration dependences of \bar{x} and T_0 ³⁶. The band offset was calculated accounting for the variation of composition profile of Mn ions in the magnetic barriers and at the interface.

The electronic structure of DMS quantum wells was found by solving Schrödinger equation for envelope functions within the effective mass approximation

$$-\frac{\hbar^2}{2} \frac{d}{dz} \left(\frac{1}{m^*(z)} \frac{d\psi(z)}{dz} \right) + \left[E_c(z) + eFz \mp \frac{1}{2} g^*(z) \mu_B B \pm \frac{1}{2} \alpha N_0 \bar{x} \langle S_z \rangle \right] \psi(z) = \left[E - \left(j + \frac{1}{2} \right) \frac{\hbar e B}{m^*} \right] \psi(z), \quad (4)$$

where \hbar is Planck constant, e is the electron charge, m^* is the electron effective mass. The second term $E_c(z)$ on the left side of Eq. 4 is the band offset, the third term is the potential due to an applied electric field F , the fourth is the potential stemming from the gyromagnetic spin splitting of Landau levels (“−” for spin-up and “+” spin-down electrons), and the fifth is the spin-dependent potential of DMS. In further considerations we will use a shorthand subscript i to denote the j_i th Landau level (LL) of the m_i th state (subband) with spin s_i , i.e. $i = |m_i, j_i, s_i\rangle$. Its energy is

$$E_i = E_{|m_i, j_i, s_i\rangle} = E_{m_i}^{s_i} + \left(j_i + \frac{1}{2} \right) \hbar \omega_c, \quad (5)$$

where $E_{m_i}^{s_i}$ is the energy of the state m_i with spin s_i , and $\omega_c = eB/m^*$ is the cyclotron frequency. The wavefunctions of all the LLs of the same spin, associated to the same state, have the same form $\psi_i(z) = \psi_{m_i}^{s_i}(z)$.

B. Interaction of electrons with electromagnetic field

In optical transitions the Landau index and spin are conserved, and absorption occurs only on transitions between LLs associated with different states. The fractional absorption of such a transition is^{13,37}

$$A_{i,f} = \frac{\pi e^2 \omega}{n \epsilon_0 c} M_{m_i, m_f}^s \delta(E_f - E_i - \hbar \omega) (n_f - n_i), \quad (6)$$

where $i = |m_i, j, s\rangle$ and $f = |m_f, j, s\rangle$ are LLs stemming from different states ($m_i \neq m_f$), E_i and E_f are their energies with the corresponding wavefunctions $\psi_{m_i}^s$ and $\psi_{m_f}^s$, $M_{m_i, m_f}^s = \int \psi_{m_f}^{s*}(z) z \psi_{m_i}^s(z) dz$ is the dipole matrix element, n_i and n_f are the electron sheet densities, n is the refraction index, ϵ_0 is the permittivity of vacuum, c is the speed of light in vacuum, and ω is the frequency of incident radiation. The fractional absorption may be written as $A_{i,f} = \sigma_{i,f} (n_i - n_f)$ with the cross-section

$$\sigma_{i,f} = \frac{\pi e^2 \omega}{n \epsilon_0 c} M_{m_i, m_f}^s \delta(E_f - E_i - \hbar \omega), \quad (7)$$

independent of the electron concentration. The total absorption between states m_i and m_f of the same spin s is a sum of contributions of all LLs stemming from them

$$A_{m_i, m_f}^s = \sum_{i, f, j_i = j_f = j, s_i = s_j = s} A_{i, f}$$

$$= \frac{\pi e^2 \omega}{n \epsilon_0 c} M_{m_i, m_f}^s \delta(E_{m_f}^s - E_{m_i}^s - \hbar \omega) \sum_{i, f, j_i = j_f = j, s_i = s_j = s} (n_f - n_i), \quad (8)$$

where $E_{m_i}^s - E_{m_f}^s = E_i - E_f$. State broadening was modeled by a Lorentzian distribution with the transition linewidth (FWHM) Γ .

C. Interaction of electrons with phonons

Within the frame of a bulk phonon model, the electron-longitudinal optical (LO) phonon scattering rate between LLs $i = |m_i, j_i, s\rangle$ and $f = |m_f, j_f, s\rangle$ if $j_i \leq j_f$ reads³⁸

$$\bar{W}_{LO}(i, f) = \frac{e^2 \omega_{LO}}{2\pi \epsilon_p} \left[n_0(\omega_{LO}) + \frac{1}{2} \mp \frac{1}{2} \right] \delta(E_i - E_f \pm \hbar \omega_{LO})$$

$$\times \int_0^\infty q_{xy} |H_{j_i, j_f}(q_{xy})|^2 dq_{xy} \int_0^\infty \frac{|G_{m_i, m_f}^s(q_z)|^2}{q_{xy}^2 + q_z^2} dq_z, \quad (9)$$

where ω_{LO} is optical phonon frequency, \mathbf{q}_{xy} ($q_{xy} = |\mathbf{q}_{xy}|$) is the xy -component and q_z is the z -component of the phonon wave vector $\mathbf{q} = (\mathbf{q}_{xy}, q_z)$, the constant ϵ_p is defined as $\epsilon_p^{-1} = \epsilon_\infty^{-1} - \epsilon_s^{-1}$ where ϵ_∞ and ϵ_s are high-frequency and static permittivity, respectively, $n_0(\omega_{LO})$ is the Bose-Einstein factor. To calculate the scattering rate if $j_i > j_f$, one swaps these indices. The upper sign in the $(n_0(\omega_{LO}) + \frac{1}{2} \mp \frac{1}{2})$ term and in the energy conservation law (the δ function) holds for absorption, and the lower sign for emission.

The form-factor $G_{m_i, m_f}^s(q_z)$ is defined as

$$G_{m_i, m_f}^s(q_z) = \int \psi_{m_f}^{s*}(z) e^{iq_z z} \psi_{m_i}^s(z) dz. \quad (10)$$

The lateral overlap integral $H_{j_i, j_f}(q_{xy})$ is given in the analytical form

$$|H_{j_i, j_f}(q_{xy})|^2 = e^{-q_{xy}^2/2\beta^2} \frac{j_i!}{j_f!} \left(\frac{q_{xy}^2}{2\beta^2} \right)^{j_f - j_i} \left[L_{j_f}^{j_f - j_i} \left(\frac{q_{xy}^2}{2\beta^2} \right) \right]^2, \quad (11)$$

where $\beta = \sqrt{\frac{m^* \omega_c}{\hbar}} = \sqrt{\frac{eB}{\hbar}}$ and $L_n^k(x)$ is the associated Laguerre polynomial. The delta function was replaced by a Gaussian³⁹ with the transition linewidth (FWHM) equal to Γ if $m_i \neq m_j$ and $j_i = j_j$, or equal to $\sigma_0 \sqrt{B} \sqrt{2 \ln 2}$ if $m_i = m_j$ and $j_i \neq j_j$, or to $\sqrt{\Gamma^2 + 2 \ln 2 \sigma_0^2 B}$

if $m_i \neq m_j$ and $j_i \neq j_j$. The parameter σ_0 is inversely proportional to the effective mass, so from its value for GaAs³⁹ (1 meV/T^{1/2}), one may estimate the value for CdMnTe.

The transition of an electron from the i th LL ($i = |m_i, j_i, s\rangle$) with larger energy than that of the final f th LL ($f = |m_f, j_f, s\rangle$) via an interaction with longitudinal acoustic (LA) phonons in a magnetic field is given by⁴⁰

$$\begin{aligned} \overline{W}_{AC}(i, f) &= \frac{D_A^2 (E_i - E_f)^2}{\pi \rho v_s^4 \hbar^3} \frac{e^{-\frac{E_i - E_f}{kT}}}{e^{\frac{E_i - E_f}{kT}} - 1} \\ &\times \int_0^{q_{zmax}} |G_{m_i, m_f}^s(q_z)|^2 |H_{j_i, j_f}(q_{xy0})|^2 dq_z, \end{aligned} \quad (12)$$

where

$$q_{xy0} = \sqrt{\left(\frac{E_i - E_f}{\hbar v_s}\right)^2 - q_z^2}. \quad (13)$$

Here D_A is the deformation potential, ρ is the density of the material, v_s the sound velocity, $G_{m_i, m_f}^s(q_z)$ and $H_{j_i, j_f}(q_{xy})$ are the form factor and the lateral overlap integral for electron-LO phonon scattering, and

$$q_{zmax} = \frac{|E_i - E_f|}{\hbar v_s}. \quad (14)$$

If $E_i < E_f$, the electron-LA scattering is calculated from a similar expression

$$\begin{aligned} \overline{W}_{AC}(i, f) &= \frac{D_A^2 (E_i - E_f)^2}{\pi \rho v_s^4 \hbar^3} \frac{1}{e^{\frac{E_i - E_f}{kT}} - 1} \\ &\times \int_0^{q_{zmax}} |G_{m_i, m_f}^s(q_z)|^2 |H_{j_i, j_f}(q_{xy0})|^2 dq_z. \end{aligned} \quad (15)$$

Generally, electron-LA scattering is less significant than electron-LO scattering.

Landau quantization and the giant Zeeman effect have a significant impact on scattering processes, enhancing or inhibiting them depending on the inter-LL energy separation. The electron-LO phonon interaction between a ground state LL and a continuum state LL increases considerably as their energy difference approaches one LO phonon energy (E_{LO}). The scattering reaches a maximum when the difference becomes equal to E_{LO} and then the corresponding LLs are in resonance. A similar conclusion applies for electron-LA phonon scattering, with the distinction that resonance occurs when two LLs have very similar energies.

D. Modeling of QWIPs in a magnetic field

A quantum mechanical model of electron dynamics in QWIPs in a magnetic field, accounting for Landau quantization and the giant Zeeman effect, was developed to describe the electron transport processes. Consider a QWIP with a large number of periods in an externally applied electric and magnetic field. The population dynamics of LLs can be obtained from the system of nonlinear rate equations in the steady state^{21,41}

$$\frac{dn_f}{dt} = 0 = \sum_{i=1, i \neq f}^{N_c} n_i W_{i,f} - n_f \sum_{i=1, i \neq f}^{N_c} W_{f,i} + \sum_{i=1, i \neq f}^{N_c} C(\Phi, n_i, n_f), \quad (16)$$

where i and f run over all N_c LLs in the cascade, in all of its periods, n_i is the electron concentration of the i th LL and $W_{i,f}$ is the total scattering rate from LL i into LL f

$$W_{i,f} = \bar{W}_{i,f} [1 - f_{FD}(E_f)], \quad (17)$$

where $\bar{W}_{i,f}$ is the scattering rate from LL i into LL f , independent of the electron distribution, and $1 - f_{FD}(E_f)$ accounts for Pauli exclusion, with f_{FD} being the Fermi Dirac function. The electron distribution over all LLs associated with some state is assumed to be Fermi Dirac-like, with electron temperature equal to the lattice temperature, but with different quasi-Fermi level E_{F,m_i} for each state m_i , i.e.

$$f_{FD}(E_i) = \frac{1}{e^{\frac{E_i - E_{F,m_i}}{kT}} - 1}, \quad (18)$$

The electron concentration on the i th LL, with energy E_i , is

$$n_i = n_{|m_i, j_i, s_i\rangle} = \frac{eB}{2\pi\hbar} f_{FD}(E_i). \quad (19)$$

The last sum in Eq. 16 is the contribution of intersubband absorption to electron transition rates with²¹

$$C(\Phi, n_i, n_f) = A_{if}(n_i, n_f)\Phi, \quad (20)$$

where A_{if} is the fractional absorption on the $i \rightarrow f$ transition, and Φ the optical flux.

Electron-LO phonon and electron-LA phonon scattering are included in the model as the main scattering mechanisms. Ionized impurity scattering is considered negligible as the doping density is assumed low. Electron-electron scattering between the ground state LLs, populated by the majority of carriers, and the LLs in the continuum is neglected because of

the relatively large energy separation, as well as between any two of the continuum state LLs because of their low population. Spin-flip scattering is in general less significant than phonon scattering⁴² and was neglected. Since the scattering between electrons of different spin is not included in the model, the rate equation system, which breaks into two independent subsystems, one for either spin orientation, together with the particle conservation law, is underdetermined. Therefore, one needs to calculate the total concentrations of spin-up and spin-down electrons. Since the perturbation of the system induced by an external electric field is relatively small, a quasiequilibrium state of the system, with a unique quasi-Fermi energy E_F , is assumed (only for calculating the total spin-up and spin-down electron concentrations). Inserting the quasi-Fermi energy E_F into Eq. 18, replacing Eq. 18 in Eq. 19 and summing over all the LLs one may obtain E_F , then find the concentrations n_i from Eq. 19 and sum those of the same spin. Hence, each electron spin subsystem is effectively described by an independent rate equation system and a particle conservation law. In this paper the simulations were carried out in the magnetic field range between 1 T and 5 T, where the population of spin-up states was found to be negligible (given in Sec. IIIB). Hence, only spin-down electron transitions were taken into account in the analysis, using only the rate equations and the particle conservation law for the spin-down electrons.

Due to the wavefunction localization properties, each state and the LLs originating from it can be associated to one of the periods of the QWIP. We assume a globally linear variation of the conduction band potential and apply the quasiperiodicity principle, i.e. if $\psi_i(z)$ is the wavefunction of a LL of energy E_i , then $\psi_i(z - D)$ is the wavefunction of a LL of energy $E_i - \Delta V$, where D is a period length and ΔV is the potential drop across a period. Therefore, by determining all the LLs (their energies and wavefunctions) belonging to one period (referred to as the central), one may obtain all the LLs in the whole structure. It is considered that a state and its LLs belong to a period if that state has a better overlap with the ground state of that period than with the ground states of the neighboring periods (overlap is here defined as the integral of their squared wavefunctions along the structure). An identical set of N states and their LLs with potentially considerable population are thus attributed to each period (high energy states are practically unpopulated). This discretization of the continuum spectrum gives an accurate description of the continuum if addition of new states and their LLs from the same basis does not affect the values of physical observables i.e. current. A LL assigned to the central period is labeled as the i th, ($i = 1, \dots, N$), and a

LL assigned to its k th nearest neighbor as the $i + kN$ th, ($i = 1, \dots, N$), where $k > 0$ for right and $k < 0$ for left neighbors. Since the interaction between LLs belonging to distant periods is negligible due to the small wavefunction overlap, the ‘tight-binding’ description is introduced, by including the interaction with only P nearest neighbors on both sides. Assuming an identical electron distribution in each period ($n_i = n_{i+kN}$), one may account explicitly for distributions in the central period, and evaluate the scattering rates within it and between any two LLs belonging to the central period and any of its P nearest neighbors on either side. Furthermore, the scattering rates are shift invariant ($W_{i,j} = W_{i+kN,j+kN}$, $W_{i-kN,j} = W_{i,j+kN}$), therefore reducing the calculation of the scattering rates by taking into account only the central period and its P right neighbors. Introducing $\alpha_B = \frac{2\pi}{eB}\hbar$ in Eq. 19 and from $A_{i,f} = \sigma_{i,f}(n_i - n_f)$ and Eq. 7, we get a system of nonlinear equations

$$\begin{aligned} \frac{dn_f}{dt} = 0 = & \sum_{i=1, i \neq f}^N n_i [\overline{W}_{i,f}(1 - \alpha_B n_f) + \sigma_{i,f}\Phi] - n_f \sum_{i=1, i \neq f}^N [\overline{W}_{f,i}(1 - \alpha_B n_i) + \sigma_{f,i}\Phi] \\ & + \sum_{k=1}^P \sum_{i=1, i \neq f}^N \{n_i [(\overline{W}_{i,f+kN} + \overline{W}_{i+kN,f})(1 - \alpha_B n_f) + (\sigma_{i,f+kN} + \sigma_{i+kN,f})\Phi] \\ & - n_f [(\overline{W}_{f+kN,i} + \overline{W}_{f,i+kN})(1 - \alpha_B n_i) + (\sigma_{f+kN,i} + \sigma_{f,i+kN})\Phi]\} \end{aligned} \quad (21)$$

where i and f run over all LLs in a period. Within the ‘tight-binding’ description, the interaction with two nearest neighbors ($P = 2$) is considered.

The current density is calculated by taking into account all electrons crossing some reference plane e.g. the interface between the central period and the adjacent right period. Effectively, this is done by subtracting the current density component due to electrons scattering through the reference plane in the direction of the potential drop from the component due to electrons scattering in the opposite direction

$$\begin{aligned} J = & \sum_{k=1}^P \sum_{i=1}^N \sum_{f=1}^N kn_i [W_{i,f+kN} - W_{i+kN,f} + (\sigma_{i,f+kN} - \sigma_{i+kN,f})\Phi] \\ = & \sum_{k=1}^P \sum_{i=1}^N \sum_{f=1}^N kn_i \left[(\overline{W}_{i,f+kN} - \overline{W}_{i+kN,f}) (1 - \alpha_B n_f) + (\sigma_{i,f+kN} - \sigma_{i+kN,f})\Phi \right] \end{aligned} \quad (22)$$

The responsivity of a QWIP is evaluated from

$$R = \frac{J(\Phi) - J(\Phi = 0)}{(hc/\lambda)\Phi}, \quad (23)$$

where λ is the detection wavelength.

III. NUMERICAL RESULTS

The design targets at simultaneously achieving maximum tunability and large oscillator strength of transitions relevant for the device operation. These clearly are the transitions of spin-down electrons from the ground state to resonant states near the barrier top⁴³. A good design should maintain the above features throughout the range of magnetic fields, from zero to where the $sp-d$ interaction saturates.

The design cycle proceeded by varying the thickness and the composition of the magnetic $\text{Cd}_{1-x}\text{Mn}_x\text{Te}$ wells and the nonmagnetic $\text{Cd}_{1-y}\text{Mg}_y\text{Te}$ barriers. Also, special care was taken to minimize the scattering rate from the ground state to the continuum, in order to minimize the dark current. This was done by tailoring the transition energies to be approximately one linewidth larger than the LO-phonon energy of the $\text{CdMnTe}/\text{CdMgTe}$ system (21 meV). The linewidth was assumed to be 30% of the transition energy of maximal strength, as is usually done in bound-continuum QWIPs⁴⁴. Solving the Schrödinger equation was implemented by a finite-difference method. Many body effects were not taken into account in the calculation due to the low doping density. The material parameters for $\text{CdMnTe}/\text{CdMgTe}$ in the electron structure computation were taken from Refs.^{45–47}. The parameters used in the scattering rate calculation were taken from Refs.^{46,48}.

A. Tunability

The designed QWIP consists of a series of 8.64 nm $\text{Cd}_{0.89}\text{Mn}_{0.11}\text{Te}$ magnetic wells and 86.4 nm $\text{Cd}_{0.855}\text{Mg}_{0.145}\text{Te}$ barriers. The doping density of the wells was chosen to be 10^{11}cm^{-2} , to satisfy the requirement for achieving relatively high absorption in the THz range at low temperatures³¹ ($\approx 0.04\%$). The temperature was set to 1.5 K, when the giant Zeeman effect is more pronounced at lower magnetic fields. The conduction band edge potential profile of the QWIP in magnetic and electric fields for spin-down electrons, together with the energies of the relevant states assigned to one period is given on the left-hand side of Fig. 1. The modification of the conduction band edge for spin-up and spin down-electrons induced by the magnetic field is shown in the right-hand side of Fig. 1.

With an applied electric field of 1 kV/cm and no magnetic field, the intersubband transition energy corresponding to the maximum oscillator strength is 26.9 meV. It increases with

magnetic field to 34.3 meV for spin-down and decreases to 19.5 meV for spin-up transitions until the $sp-d$ exchange interaction saturates at $B = 5$ T, Fig. 2. With this design, the energy range of 19.5 – 24.1 meV is not accessible because of the small population of spin-up electrons for magnetic fields of 1 – 5 T (explained below), effectively limiting the tuning range to 24.1 – 34.3 meV.

The contribution of other continuum states to the responsivity slightly shifts the peak detection energy upwards. For magnetic fields of 1 – 5 T, for spin-down transitions, the peak detection energy differs from the transition energy of maximal strength up to 1.5 meV, maintaining the tunability obtained from the consideration of the maximal strength transitions. It is expected that this conclusion also applies for both the spin-up and spin-down transitions in magnetic fields of 0 – 1 T.

B. Population of Landau levels

The population of LLs, especially those stemming from the ground state, determines the QWIP output characteristics, such as current and responsivity. Therefore, the discussion of the LL population is given first.

The energies of several lowest index LLs originating from the ground and the first continuum state of both the spin-up and spin-down subsystems, and the quasi-Fermi level E_F vs. magnetic field dependences are given in Fig. 3. The inset of Fig. 4 shows the distribution of spin-up and spin-down electrons in a magnetic field from 1 T to 5 T. At magnetic fields above 1 T the LL configuration is such that all the LLs of spin-up electrons are above E_F . Given that the temperature is near zero, the population of these levels is extremely small, and so is their contribution to the absorption and scattering processes. For spin-down electrons some low index LLs of the ground state are below E_F and hence most of the electrons reside there. Therefore, only spin-down electrons contribute to transport processes. This phenomenon represents the spin-polarization of the system.

The distribution of a few lowest ground state LLs of spin-down electrons, calculated from the rate equation model as a function of magnetic field, is given in Fig. 4. The decrease of the LL population occurs at the same magnetic fields where Fermi energy drops, justifying the assumption that the system is close to equilibrium, which was introduced to calculate the concentration of spin-up and spin-down electrons.

C. Dark current

The population in the continuum is mainly determined by the transitions between the ground LLs and the continuum, and the magnetic field influence on the scattering between continuum LLs is of secondary importance. Hence, the dark current is determined by scattering from the populated ground state LLs, from which the electrons are injected into the continuum. Therefore, scattering from the ground state LLs is considered first.

The average scattering rate from the ground state LLs to the continuum is defined as

$$W_i^a = \frac{n_i \sum_{f, m_f \neq 1} W_{i,f}}{\sum_{f, m_f=1} n_f} \approx \frac{n_i}{n_s} \sum_{f, m_f \neq 1} W_{i,f}, \quad (24)$$

where $i = |1, j_i, -1/2\rangle$, $j_i \geq 0$, is a ground state LL, n_s is the doping density and it is assumed that the continuum LL population is small. These are shown in Fig. 5 as functions of the magnetic field, for an electric field of 1 kV/cm. At a fixed electric field, an increasing magnetic field causes the energy separation between any of the ground state LLs except the lowest ($|1, j_i\rangle$, $j_i > 0$), and the continuum to decrease towards E_{LO} , significantly enhancing the corresponding scattering rates. On the other hand, the separation between the ground state and the continuum states increases, and becomes more distant from E_{LO} , which results in a reduction of the scattering rate from the $|1, 0\rangle$ LL to the continuum. However, since the ground state–continuum transition energies are remote from E_{LO} in the whole range of magnetic fields (a requirement in the design), this decrease does not have a large effect on scattering from $|1, 0\rangle$. Since the concentration of each ground state LL increases and then decreases (apart from $|1, 0\rangle$ which increases and reaches saturation), see Fig. 4, all average scattering rates increase until the decrease of concentration prevails, causing their decrease with further increase of magnetic field, as shown in Fig. 5. The described maxima in $|1, 1\rangle$, $|1, 2\rangle$, $|1, 3\rangle$ occur at magnetic fields of 3.5 T, 1.8 T and 1.2 T, respectively, in Fig. 5. The other peaks in the average scattering rates of $|1, 2\rangle$ and $|1, 3\rangle$ in Fig. 5 appear as the consequence of their resonances with some of continuum LLs, when the scattering rates become strongly enhanced and prevail over the effects of decreasing population.

The dark current vs. magnetic field dependence is shown in Fig. 6. From Fig. 5 and Fig. 6 one can see that the dark current follows the same trend as the total average scattering rate from all the ground state LLs. Since only spin-down electrons here interact with phonons, the dark current is spin-down-polarized. The zero-field extrapolation of the results from our

model shows a reasonable agreement with the measured values of the dark current in the first reported bound-continuum THz QWIP³¹, as well as in another, just published, structures³², for the identical value of electric field (1 kV/cm).

The dark current/electric field characteristics at $B = 3$ T is shown in the inset of Fig. 6. Applying a stronger electric field causes an increase of dark current, just as in QWIPs without magnetic field. This is because the applied electric field does not affect the LL configuration, so despite the discretization of the spectrum this system behaves similarly to the one having simple parabolic dispersion in the plane of the layers.

D. Responsivity

The population of higher index ground state LLs decreases with magnetic field, and hence, so does the number of photoelectrons generated from them into higher index continuum states LLs, see Fig. 4. In contrast, the population of low index ground state LLs and of photoelectrons generated from them into low index continuum states LLs increase. The contribution of higher index LLs photoelectrons to the photocurrent is larger than that of low index LLs photoelectrons, because of their larger transition rates to the neighboring periods. Therefore, the responsivity generally exhibits a decreasing dependence on the magnetic field, shown in Fig. 7. However, this trend is changed when an increasing number of photoelectrons in low index continuum LLs becomes more important than the decreased number of higher index continuum LLs photoelectrons, and then the responsivity increases. The scattering rates from the continuum to the ground state LLs increase with the magnetic field because the energy spacing between relevant LLs approaches E_{LO} . The responsivity vs. magnetic field dependence is again reversed, reaching a maximum in Fig. 7, when scattering rates from low index continuum LLs increase sufficiently to reduce photoelectron concentration on them. The responsivity then continues to follow the general trend. Photocurrent is spin-down polarized because only the spin-down electron transitions occur via the interaction with phonons and incident radiation. In comparison to previously reported bound-continuum THz QWIPs^{31,32}, at 1 kV/cm the order of magnitude of the responsivity in the whole range of magnetic fields is the same (~ 0.1 A/W).

The inset of Fig. 7 shows the responsivity as a function of bias for $B = 3$ T. At a fixed magnetic field, the bias dependence of responsivity is qualitatively the same as in QWIPs

with no magnetic field.

IV. CONCLUSION

A quantum mechanical model of electron transport in QWIPs in magnetic field was developed and used to design and analyze the performance of magnetic field tunable DMS THz QWIPs. The tunability is based on the magnetically induced variation of the band offset potential profile. The QWIP parameters were engineered to get maximal tunability in the desired range of the far infrared spectrum, while maintaining low dark current and large responsivity. The values of current density and responsivity were calculated and found to be of the same order of magnitude as in GaAs/AlGaAs THz QWIPs.

Acknowledgment

The authors would like to thank the European Office of Aerospace Research and Development for funding under contract FA8655-04-1-3069.

-
- ¹ N. Samarth, *Solid State Phys* **58**, 1 (2004).
- ² H. Akinaga, H. Ohno, *IEEE T Nanotechol* **1**, 19 (2002).
- ³ T. Dietl, *J. Magn. Magn. Mater.* **272**, 1969 (2004).
- ⁴ H. Ohno, *Science* **281**, 951 (1998).
- ⁵ J. K. Furdyna, *J. Appl. Phys.* **64**, R29 (1988).
- ⁶ J. A. Gaj, in *Diluted Magnetic Semiconductors*, edited by J. K. Furdyna and J. Kossut, *Semiconductors and Semimetals*, Vol. 25 (Academic, Boston, 1988), Chap. 7.
- ⁷ T. Wojtowicz, M. Kutrowski, G. Karczewski, J. Kossut, *Appl. Phys. Lett.* **73**, 1379 (1998).
- ⁸ I. A. Merkulov, D. R. Yakovlev, A. Keller, W. Ossau, J. Geurts, A. Waag, G. Landwehr, G. Karczewski, T. Wojtowicz, J. Kossut, *Phys. Rev. Lett.* **83**, 1431 (1999).
- ⁹ S. Lee, M. Dobrowolska, J. K. Furdyna, H. Luo, L. R. Ram-Mohan, *Phys. Rev. B* **54**, 16939-16951 (1996).
- ¹⁰ M. Syed, G. L. Yang, J. K. Furdyna, M. Dobrowolska, S. Lee, L. R. Ram-Mohan, *Phys. Rev. B* **66**, 075213 (2002).
- ¹¹ E. D. Isaacs, D. Heiman, J. J. Zayhowski, R. N. Bicknell, J. F. Schetzina, *Appl. Phys. Lett.* **48**, 275 (1986).
- ¹² Y. Yamada, Y. Masumoto, J. T. Mullins, T. Taguchi, *Appl. Phys. Lett.* **61**, 2190 (1992).
- ¹³ I. Savić, V. Milanović, Z. Ikonić, D. Indjin, V. Jovanović, P. Harrison, *IEEE J. Quantum Electron.* **40**, 1614 (2004).
- ¹⁴ A. Rogalski, *J. Appl. Phys.* **93**, 4355 (2003).
- ¹⁵ J. Faist, D. Hofstetter, M. Beck, T. Aellen, M. Rochat, S. Blaser, *IEEE J. Quant. Electron.* **38**, 533 (2002).
- ¹⁶ L. Jiang, S. S. Li, M. Z. Tidrow, W. R. Dyer, W. K. Liu, J. M. Fastenau, T. R. Yurasits, *Appl. Phys. Lett.* **79**, 2982 (2001).
- ¹⁷ M. Z. Tidrow, X. Jiang, S. S. Li, K. Bacher, *Appl. Phys. Lett.* **74**, 1335 (1999).
- ¹⁸ H. C. Liu, R. Dudek, A. Shen, E. Dupont, C. Y. Song, Z. R. Wasilewski, M. Buchanan, *Appl. Phys. Lett* **79**, 4237 (2001).
- ¹⁹ L. Gendron, M. Carras, A. Huynh, V. Ortiz, C. Koeniguer, V. Berger, *Appl. Phys. Lett.* **85**, 2974 (2004).

- ²⁰ V. Ryzhii, M. Ryzhii, H. C. Liu, J. Appl. Phys. **92**, 207 (2002).
- ²¹ V. D. Jovanović, P. Harrison, Z. Ikonić, D. Indjin, J. Appl. Phys. **96**, 269 (2004).
- ²² J. L. Pan, C. G. Fonstad, IEEE J. Quant. Electron. **35**, 1673 (1999).
- ²³ L. Thibaudeau, P. Bois, J. Y. Duboz, J. Appl. Phys. **79**, 446 (1996).
- ²⁴ S. D. Gunapala, S. V. Bandara, J. K. Liu, E. M. Luong, N. Stetson, C. A. Shott, J. J. Bock, S. B. Rafol, J. M. Mumolo, M. J. McKelvey, IEEE Trans. Electron. Dev. **47**, 326 (2000).
- ²⁵ S. D. Gunapala, S. V. Bandara, A. Singh, J. K. Liu, S. B. Rafol, E. M. Luong, J. M. Mumolo, N. Q. Tran, D. Z.-Y. Ting, J. D. Vincent, C. A. Shott, J. Long, P. D. LeVan, IEEE Trans. Electron. Dev. **47**, 963 (2000).
- ²⁶ R. Köhler, A. Tredicucci, F. Beltram, H. E. Beere, E. H. Linfield, A. G. Davies, D. A. Ritchie, R. C. Iotti, F. Rossi, Nature **417**, 156 (2002).
- ²⁷ M. Rochat, L. Ajili, H. Willenberg, J. Faist, H. E. Beere, A. G. Davies, E. H. Linfield, D. A. Ritchie, Appl. Phys. Lett. **81**, 1381 (2002).
- ²⁸ B. S. Williams, H. Callebaut, S. Kumar, Q. Hu, J. Reno, Appl. Phys. Lett. **82**, 1015 (2002).
- ²⁹ J. Alton, S. Barbieri, J. Fowler, H. E. Beere, J. Muscat, E. Linfield, D. A. Ritchie, G. Davies, R. Köhler, A. Tredicucci, Phys. Rev. B **68**, 081303 (R) (2003).
- ³⁰ M. Graf, G. Scalari, D. Hofstetter, J. Faist, H. Beere, E. Linfield, D. Ritchie, G. Davies, Appl. Phys. Lett. **84**, 475 (2004).
- ³¹ H. C. Liu, C. Y. Song, A. J. SpringThorpe, J. C. Cao, Appl. Phys. Lett. **84**, 4068 (2004).
- ³² H. Luo, H. C. Liu, C. Y. Song, Z. R. Wasilewski, Appl. Phys. Lett. **86**, 231103 (2005).
- ³³ C. Becker, C. Sirtori, O. Drachenko, V. Rylkov, D. Smirnov, J. Leontin, Appl. Phys. Lett. **81**, 2941 (2002).
- ³⁴ D. Smirnov, O. Drachenko, J. Leontin, H. Page, C. Becker, C. Sirtori, V. Apalkov, T. Chakraborty, Phys. Rev. B **66**, 125317 (2002).
- ³⁵ L. D. Landau, E. M. Lifshitz, *Quantum Mechanics: Nonrelativistic Theory* (Pergamon, London, 1959).
- ³⁶ J. A. Gaj, W. Grieshaber, C. Bodin-Deshayes, J. Cibert, G. Feuillet, Y. Merle d'Aubigne, A. Wasiela, Phys. Rev. B **50**, 5512 (1994).
- ³⁷ S. Živanović, V. Milanović, Z. Ikonić, Phys. Rev. B **52**, 8305 (1995).
- ³⁸ P. J. Turley, S. W. Teitworth, J. Appl. Phys. **72**, 2356 (1993).
- ³⁹ J. Eisenstein, H. Stormer, V. Narayanamurti, A. Cho, A. Gossard, C. Tu, Phys. Rev. Lett.

- 55**, 875 (1985).
- ⁴⁰ G. Sun, J. B. Khurgin, IEEE J. Quantum Elect. **29**, 1104 (1993).
- ⁴¹ Z. Ikonić, P. Harrison, R. W. Kelsall, J. Appl. Phys. **96**, 6803 (2004).
- ⁴² A. Dyson, B. K. Ridley, Phys. Rev. B **69**, 125211 (2004).
- ⁴³ K. K. Choi, *The Physics of Quantum Well Infrared Photodetectors*, Series in Modern Condensed Matter Physics, Vol. 7 (World Scientific, Singapore), p. 130-148.
- ⁴⁴ B. F. Levine, J. Appl. Phys. **74**, R1 (1993).
- ⁴⁵ T. Lebihen, E. Deleporte, C. Delalande, Phys. Rev. B, **55**, 1724, (1997).
- ⁴⁶ E. Oh, C. Parks, I. Miotkowski, M. Dean Sciacca, A. J. Mayur, A. K. Ramdas, Phys. Rev. B **48**, 15040 (1993).
- ⁴⁷ Y. H. Matsuda, T. Ikaida, N. Miura, S. Kuroda, F. Takano, K. Takita, Phys. Rev. B **65**, 115202 (2002).
- ⁴⁸ *Numerical Data and Functional Relationship in Science and Technology*, edited by K. H. Hellwege, Landolt-Börnstein, New Series, Group III, Vol. 17, Pt. b (Springer-Verlag, Berlin,1982), p. 225-228.

Figure captions

FIG. 1: Left-hand side: The conduction band profile of the QWIP, the energies of states that belong to one period (dashed lines) and the squared wavefunctions of the ground state and the continuum state with maximal oscillator strength towards the ground state, for the electric field $E = 1$ kV/cm and magnetic field $B = 5$ T. Right-hand side: The conduction band profile in a magnetic well and in the vicinity of interfaces: for both spins at $B = 0$ T (solid line), for spin-up electrons at $B = 5$ T (dashed line) and for spin-down electrons at $B = 5$ T (dash-dotted line).

FIG. 2: Transition energies corresponding to maximal oscillator strength for spin-down and spin-up electrons vs. magnetic field dependence, at a fixed electric field of 1 kV/cm.

FIG. 3: The fan-out of Landau levels from the ground and the first continuum states for both the spin-up and spin-down electron system, together with the quasi-Fermi level, for a fixed electric field of 1 kV/cm.

FIG. 4: The electron distribution over the first 4 ground state Landau levels vs. magnetic field dependence at a fixed electric field of 1 kV/cm. Inset: the electron distributions over the spin-up and spin-down states vs. magnetic field dependence for the same electric field.

FIG. 5: Average scattering rates (see text for explanation) from the first 4 ground state Landau levels to the continuum, and the total average scattering rate from all ground state Landau levels vs. magnetic field dependence at a fixed electric field of 1 kV/cm.

FIG. 6: Dark current density vs. magnetic field dependence for a fixed electric field of 1 kV/cm. Inset: dark current density vs. electric field dependence for a fixed magnetic field of 3 T.

FIG. 7: Responsivity vs. magnetic field dependence for a fixed electric field of 1 kV/cm. Inset: responsivity vs. electric field dependence for a fixed magnetic field of 3 T.

Figures

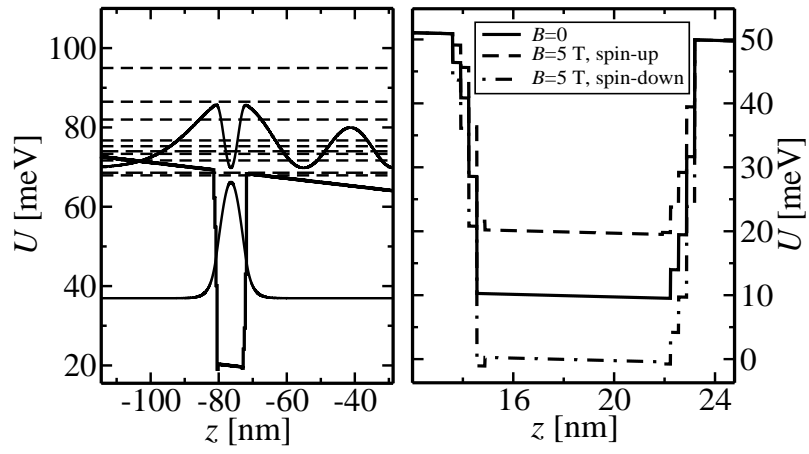


FIG. 1:

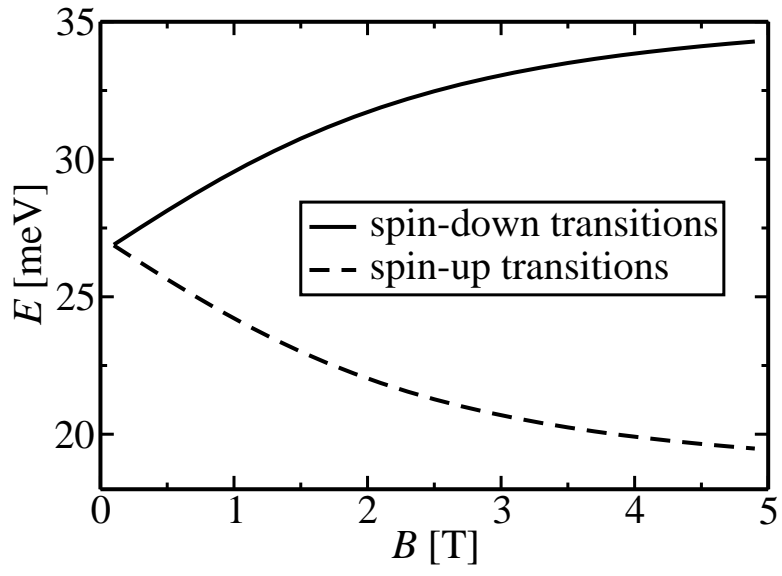


FIG. 2:

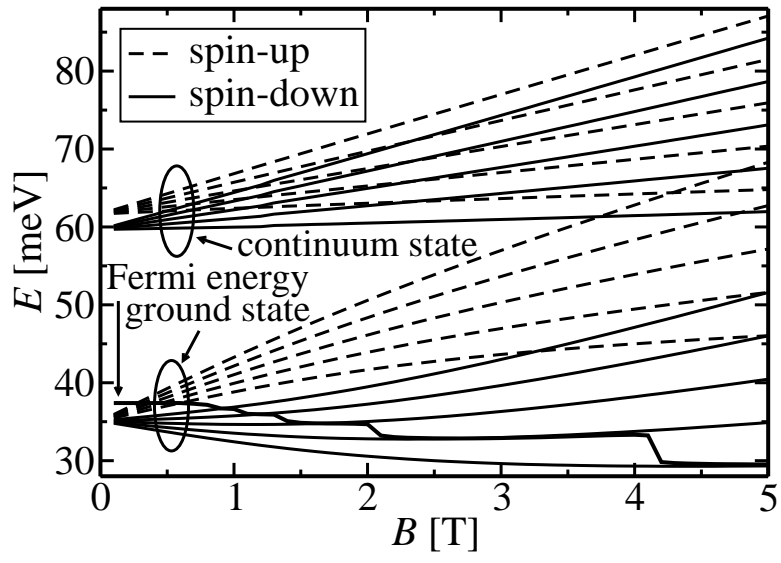


FIG. 3:

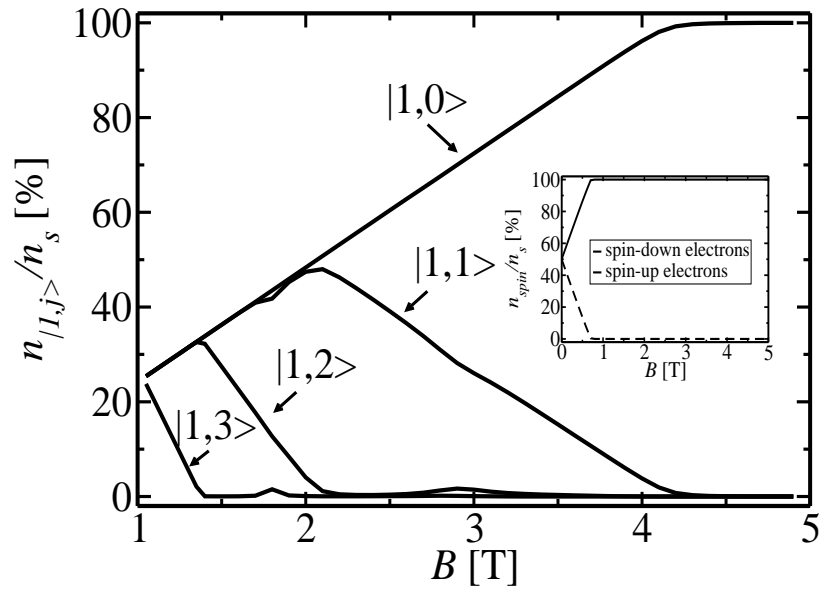


FIG. 4:

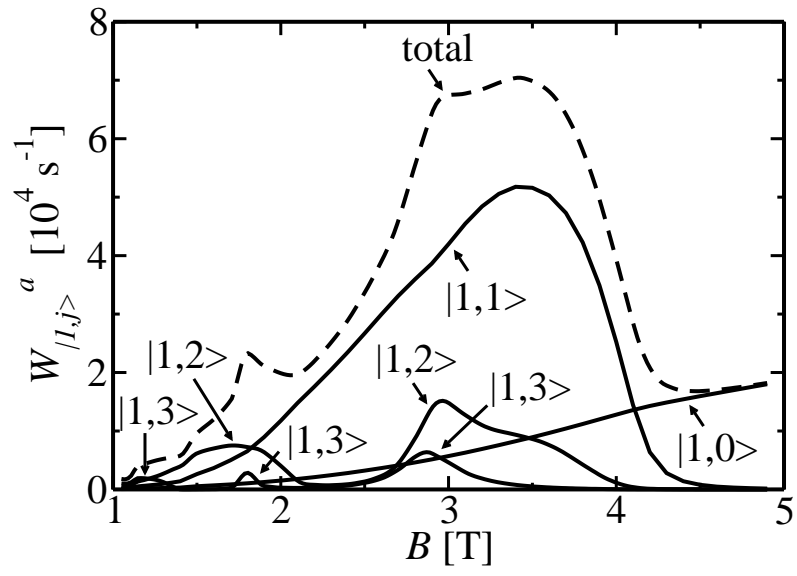


FIG. 5:

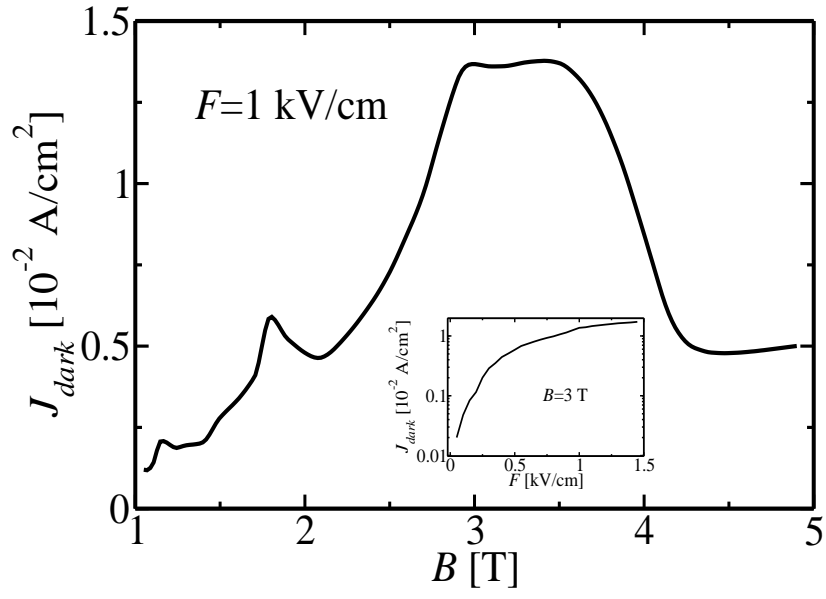


FIG. 6:

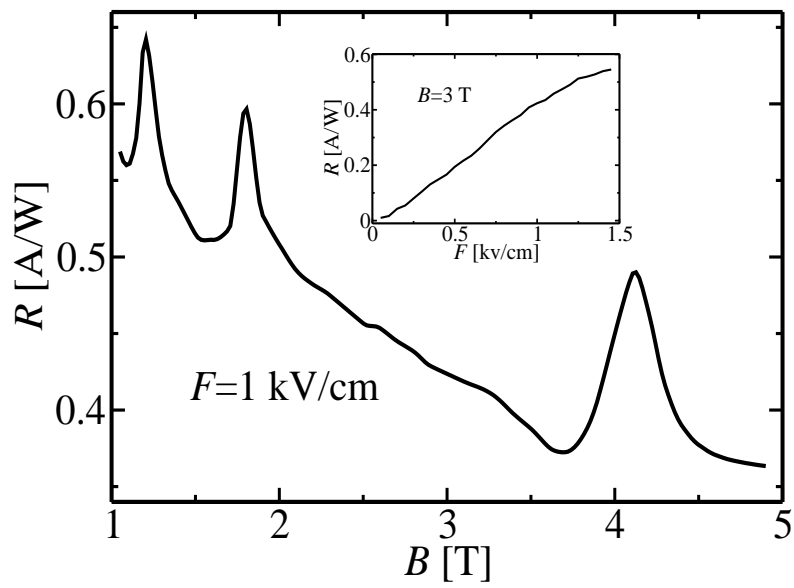


FIG. 7: